Journal of Alloys and Compounds xxx (xxxx) xxx

Contents lists available at ScienceDirect

Journal of Alloys and Compounds

journal homepage: http://www.elsevier.com/locate/jalcom

A study of the cycle oxidation behavior of the Cr/Mn/Mo alloyed Ti–48Al–based intermetallics prepared by ECAS

Y. Garip, O. Ozdemir*

Sakarya Applied Science University, Technology Faculty, Department of Metallurgy and Materials Engineering, Esentepe Campus, 54187, Sakarya, Turkey

ARTICLE INFO

Article history:
Received 6 August 2019
Received in revised form
24 October 2019
Accepted 27 October 2019
Available online xxx

Keywords:
Ti-Al
Aluminides
Oxidation
Powder metallurgy
Sintering

ABSTRACT

Today the electric current activated sintering (ECAS) technique is commonly preferred as it has many advantages such as microstructure control, reduction of process time, rapidly heating rate and sintered parts with full density. Two-phased (α_2-Ti_3Al+γ-TiAl) TiAl alloys have drawn considerable interest for automotive, aerospace and gas turbine industry applications because of their low density and superior high-temperature properties. The study aims to investigate the effect of the alloying elements (Cr, Mn, Mo) on the oxidation resistance of TiAl based intermetallics produced by ECAS under the cyclic condition. The cycle oxidation behavior of two-phased intermetallics in air at 700, 800 and 900 °C for 180 h was studied. The phase composition, microstructure, surface morphology and cross-sectional microstructure of the specimens were examined using SEM, EDS and XRD. According to the XRD and EDS results, the formed scale was composed mainly of TiO_2 and Al_2O_3 phases. The cross-section SEM images show that the oxide scales of the alloys featured strong adhesion of scale with a multi-layered structure. The scales on the Mo-added alloys are thinner, compact and adherent and thus the scale-exfoliation resistance is enhanced. The activation energy values calculated for the oxidation of specimens varied between 50 and 116 kJ mol^{-1}. Considering the thermodynamic and kinetic factors, possible oxidation mechanism of studied specimens was discussed.

1. Introduction

TiAl-based intermetallics are very interesting materials for automotive, aerospace and gas turbine industry applications as they have superior properties such as low density (3.9–4.2 g cm^{-3}), good creep resistance, high specific strength, high Young's modulus, high rigidity at high temperatures, high melting temperature and good oxidation resistance. Moreover, TiAl based intermetallics have superior oxidation feature than conventional Ti alloys. These intermetallics are also regarded as an alternative material to Ni-based superalloys, which are used in turbine engines and are about twice as dense. The replacement of nickel-based materials of gas turbines with TiAl-based alloys will cause a decrease in NOx emissions (80%), weight (20–30%), noise (50%), and fuel consumption (20%) [1–9]. Although TiAl-based intermetallic alloys have great potential for structural application, the problem of low ductility (1–2%) and fracture toughness (10–25 MPa $m^{1/2}$) at room temperature are major problems [9,10]. Another factor limiting the application area is that these alloys do not have good oxidation above 800 °C since the external layer of the oxide scale is composed of TiO_2 or TiO_2 and Al_2O_3 rather than a protective Al_2O_3 layer [11–13]. It was reported that the ternary and quaternary alloying elements significantly affect the oxidation resistance of TiAl intermetallics [10,11,14]. The Mn, V and Cr elements have the effect of decreasing the grain size of TiAl based alloys and thus cause improvement in ductility. However, it has been postulated that these elements decrease the oxidation resistance of the alloys [11,12]. Alloying elements of Nb, Mo, W and Si provide an important contribution to enhance the oxidation resistance of these intermetallics [10,12,14,15]. Positive effects of Mo and Nb are explained concerning doping effect. Additionally, these elements increase the diffusion and thermodynamic activity of Al [10]. The doping effect means the reduction of oxygen vacancies which provide oxygen diffusion in the rutile lattice by alloying elements of higher valences than Ti, such as Nb and W, and as a result of this, TiO_2 growth is suppressed [10,12].

Powder metallurgy (PM), investment casting and ingot metallurgy (IM) are the widespread processes used in the production of TiAl parts. The powder metallurgy process overcomes most

* Corresponding author.
E-mail address: oozdemir@sakarya.edu.tr (O. Ozdemir).

https://doi.org/10.1016/j.jallcom.2019.152818
0925-8388/

problems such as inhomogeneity, varying microstructure, centerline porosity and density differences that occur in ingot metallurgy [8]. The electric current activated sintering (ECAS) process is a synthesizing technique in which the mechanical load is exerted simultaneously with electric current passing through loose powders by being put in a die or a cold formed compact. In this method, heat is generated as a result of electrical current passing through a resistant material based on a joule effect. Furthermore, the ECAS method has superior properties compared to conventional sintering methods such as hot pressing or pressureless sintering. This method has many advantages, including lower processing temperature, shorter sintering time, faster heating rate, the elimination of the need of sintering aids, lesser sensitivity to the feature of the starting powders and the synthesized materials with a density close to theoretical one [16–18]. The oxidation studies of TiAl intermetallics fabricated by various methods, such as vacuum arc melting [1,2,4,19,20], induction melting [10,12] and HIP [14,21] have been found in the literature. However, it was determined that very little work has been done on the oxidation of these materials prepared by ECAS technique.

The cyclic oxidation test was preferred to simulate the conditions in the gas turbine environment. The cyclic test is more aggressive than isothermal test because of the thermal shocks. It is known that a material can suffer from thermal contraction during cooling while it exposures thermal expansion during heating [22]. This causes the thermal expansion mismatch between the matrix and oxide scale, hence, the exfoliation of the oxide scale will cause further oxidation of the alloy. The obtained findings in this study can be expected to provide a reference for the investigate of TiAl based alloys' oxidation behavior.

2. Materials and methods

2.1. Materials preparation

The TiAl based intermetallics with a nominal composition of (at.%) Ti–48Al, Ti–48Al–2Cr, Ti–48Al–2Mn, Ti–48Al–2Cr–1Mo and Ti–48Al–2Mn–1Mo were synthesized by ECAS process. The powders included Ti (99.5%, size 40 μm), Al (99.5%, size 10 μm), Cr (99.8%, size 5 μm) Mo (99.9%, size 3 μm) and Mn (99.6%, size 10 μm).

In order to obtain a homogenous powder mixture for milling the powders, a stainless steel cylinder including stainless steel balls was used. The weight ratio of balls to powders was 5:1, the rotation speed of ball milling was 200 r/min and milling duration was 4 h. A 6 g powder mixture was filled in a steel die (internal dia. of 20 mm). The mixed powders were pressed under a uniaxial 60 MPa load in the steel die for 1 min. The compact was synthesized by application of a working pressure of 80 MPa at 4200 A for 35 min in the air via ECAS. The sintering pressure was kept through the process. As the voltage could be set by a controller, the optimal temperature cycle was provided during synthesizing. After synthesizing, the specimen inside the steel die was removed using uniaxial pressure and then air cooled. The flowchart of the experimental study was shown in Fig. 1. The size of the specimen was 20 mm in dia. and thickness of 4 mm (Fig. 1).

2.2. Cyclic oxidation test

The original surface area of each specimen was identified with the Solidworks before cyclic oxidation test, and then they were weighed by a digital electronic balance with an accuracy of 10^{-5} g. The oxidation tests were conducted in an electric resistance furnace at 700, 800 and 900 °C with 15 cycles up to 180 h. Each cycle consisted of heating the specimens to working temperature, holding it for 12 h in the furnace, the specimens were removed from it and finally it was air cooled. For each cycle, the weight changes of the specimens were measured. The measured weights were recorded after each cycle to assess the oxidation kinetics of the specimens. Furthermore, two measurements were carried out for each cycle, averaged and then recorded. Afterwards the specimens were again replaced to the furnace for exposure. The procedure was repeated up to the end of the cycle oxidation study.

2.3. Characterization

Prior to the SEM observation, the synthesized specimens were prepared by the classic metallographic method. The relative densities of the synthesized specimens were found by the Archimedes' technique. The microhardness of the specimens was determined by a microhardness tester equipped with a Vickers diamond pyramid indenter. For each specimen, 5 measurements were performed using the application of a load of 100 g for a dwell time of 10 s and then was recorded the average of five measurements. In order to examine the microstructures of the synthesized specimens, they were etched with Kroll's reagent.

The present phases of the specimens after the oxidation were identified by XRD (RIGAKU) analysis with Cu Kα radiation. The XRD data scanning angle 2-theta range from 10° to 90° with a step size of 0.02°. For imaging and analyzing the surface morphology of oxidation products and the cross-sectional microstructure of the oxidized specimens were employed by SEM (JEOL) and also energy-dispersive spectroscopy (EDS) was used for microanalysis.

3. Results and discussion

3.1. Initial microstructure

The chemical reactions that may take place between Ti and Al during sintering process are given below:

$$Ti + 3Al = TiAl_3 \quad (1)$$

$$4Ti + TiAl_3 = 2TiAl + Ti_3Al \quad (2)$$

In the first step, Ti and Al form the $TiAl_3$ phase, the intermediate product, by reacting below the melting temperature of Al (~600 °C). As illustrated in Fig. 2, at all temperatures, $TiAl_3$ has the lowest free energy compared to TiAl and Ti_3Al intermetallic phases. For instance, at 750 K, the difference in the Gibbs free energy of formation of $TiAl_3$ in comparison with TiAl and Ti_3Al was 10×10^3 and 7×10^3 J mol^{-1}, respectively (Fig. 2). The free energy of formation of other intermetallic compounds in the Ti–Al system can be found in Ref. [23]. Therefore, the first intermetallic phase to be formed during sintering will be $TiAl_3$. In addition, the higher diffusion rate of Al in $TiAl_3$ than other intermetallic phases makes this phase more stable at low temperatures [24]. Moreover, Al melts during sintering and this increases the diffusion rate [25]. It should be noted that the Reaction 1 is highly exothermic, which can cause some local superheating [24]. In the second step (Reaction 2), TiAl and Ti_3Al phases are formed as a result of the reaction between Ti (remaining) and $TiAl_3$ at high temperatures. When the above reactions were induced, $TiAl_3$ intermediate phase layer formed along the Ti/Al phase boundary and a TiAl intermediate phase layer formed along the Ti/$TiAl_3$ phase boundary [26].

In our study, the formation of TiAl and Ti_3Al phases with respect to the Reactions (1–2) was confirmed by XRD analysis (Fig. 3). This suggests that the phase development sequence in the Ti–Al system was not changed by the application of electric current during the ECAS process. It was observed that it is consistent with the reports

Please cite this article as: Y. Garip, O. Ozdemir, A study of the cycle oxidation behavior of the Cr/Mn/Mo alloyed Ti–48Al–based intermetallics prepared by ECAS, Journal of Alloys and Compounds, https://doi.org/10.1016/j.jallcom.2019.152818

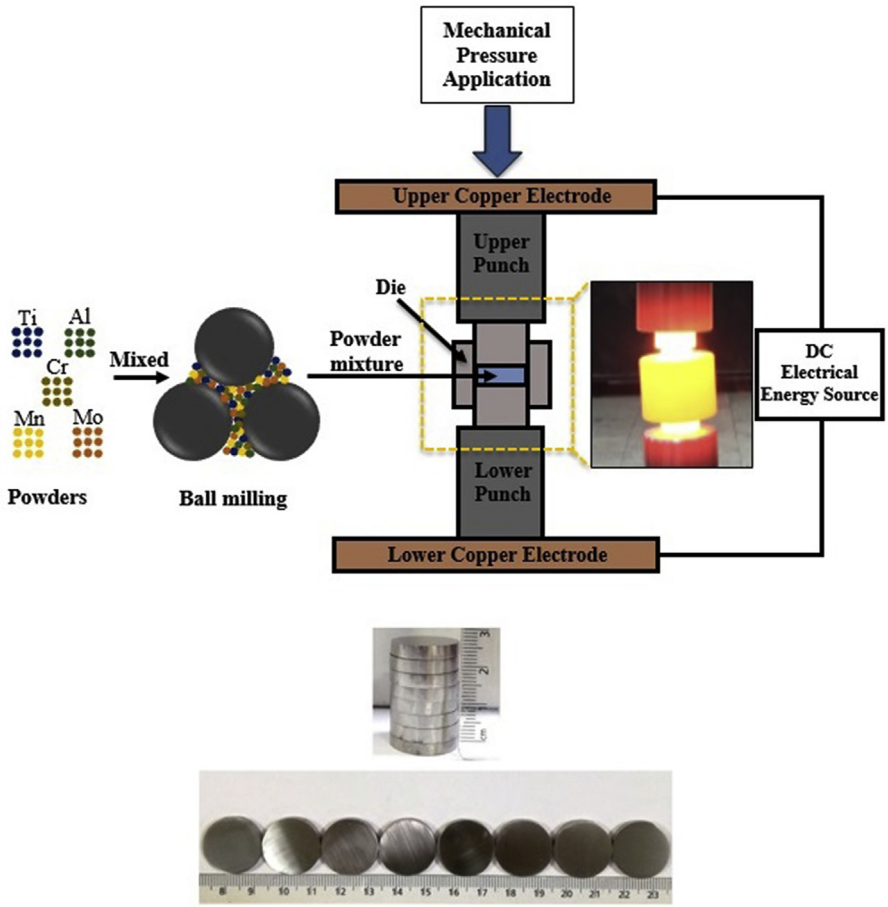

Fig. 1. The flowchart of the experimental study and sizes of synthesized specimens.

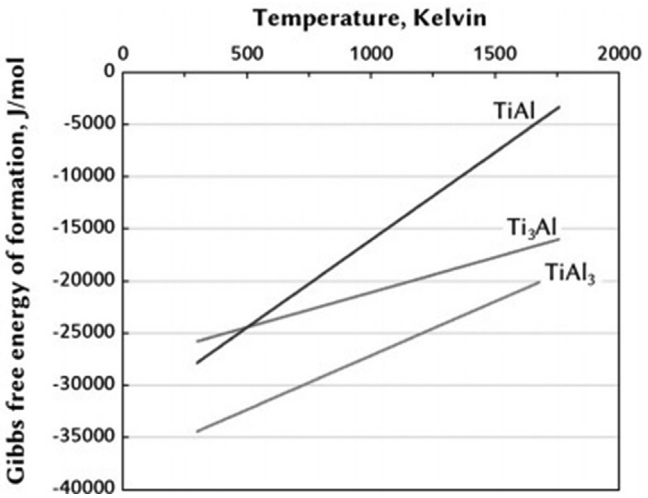

Fig. 2. Gibbs free energy of formation of the TiAl intermetallic phases as a function of temperature [25].

in Ref. [26]. Considering the fact that $TiAl_3$ phase could not be detected by XRD, this indicates that the applied current and sintering time were sufficient during ECAS.

Tamburini et al. [27] investigated the electric current influence on the growth kinetics of the product phase in Mo–Si system. They observed a significant increase in the rate of growth when applying the electric current. It was reported that growth kinetics of the intermetallic phases were increased by the applied current [26]. However, the current direction had no effect on the diffusion kinetics of the reaction [27]. It was found that the applied current promoted the nucleation of the product phases and increased the growth kinetics and reactivity in solid–solid interfacial reactions [26–28].

As shown in Fig. 3, the intermetallic alloys consist of α_2-Ti_3Al and γ-TiAl phases. It was seen from the XRD analyzes that the alloying elements did not change the phase composition. However, the elements Cr and Mn shifted the TiAl phase to larger 2θ values (see inset in Fig. 3), suggesting a decrease in TiAl lattice constant. Since Cr (0.185 nm) and Mn (0.179 nm) have smaller atomic radii than Ti (0.200 nm), the substitution of the atoms of these elements by the Ti atom causes lattice shrinkage. It can be expressed by Bragg law; $n\lambda = 2d\sin(\theta)$, when λ is constant, as the lattice constant decreases, the lattice spacing d decreases, leading to an increase in diffraction angle (θ). Although there was no significant difference between the Mo (0.201 nm) and Ti atomic radii, the peak position of the TiAl phase in Mo-added intermetallic shifted to smaller 2θ values and an enlargement occurred in the TiAl lattice.

It was reported by Liu et al. that a two-phase ($\gamma+\alpha_2$) microstructure was obtained by sintering the material having composition of at.% Ti–48Al using vacuum heat treatment for 2 h at 1200 °C [25]. In another study, Couret et al. [29] sintered Ti–47Al–2Cr–2Nb and Ti–44Al–2Cr–2Nb–1B alloys in a temperature range of 1100–1250 °C using the spark plasma sintering (SPS) method and they reported that two-phase ($\gamma+\alpha_2$) duplex and lamellar microstructures occurred during the process. Considering the cost of SPS

Please cite this article as: Y. Garip, O. Ozdemir, A study of the cycle oxidation behavior of the Cr/Mn/Mo alloyed Ti–48Al–based intermetallics prepared by ECAS, Journal of Alloys and Compounds, https://doi.org/10.1016/j.jallcom.2019.152818

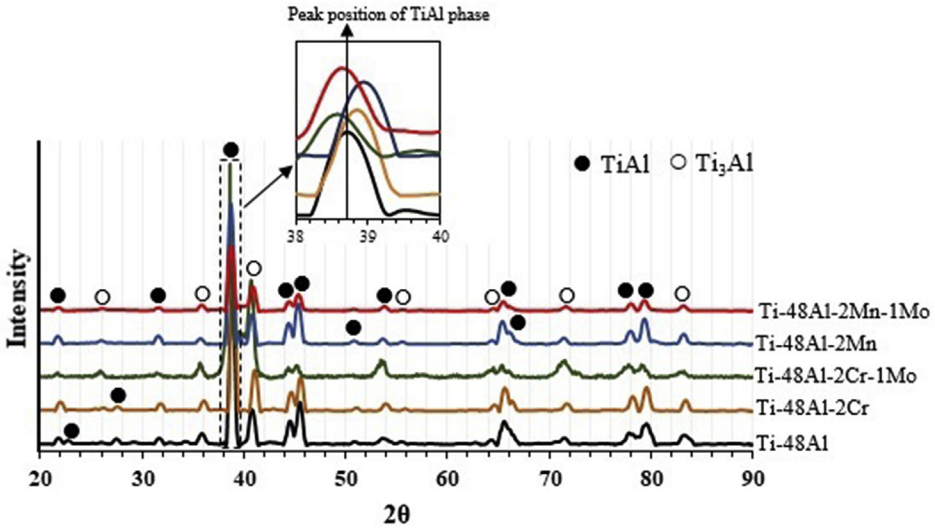

Fig. 3. XRD patterns of TiAl based alloys prepared by ECAS.

technology, materials consisting of the same phases ($\gamma+\alpha_2$) were produced in this study by the ECAS method with lower cost. SEM images of TiAl-based intermetallics synthesized by ECAS are shown in Fig. 4. EDS analysis was performed to identify different phase regions in microstructures. The chemical compositions (at. %) of spots displayed in Fig. 4 are listed in Table 1.

It was monitored from the SEM images of Ti−48Al, Ti−48Al−2Cr and Ti−48Al−2Mn intermetallic that the microstructures have consisted of two different phase regions as light and dark color. However, in specimens with Mo additions, a bright phase was detected in addition to these phases. According to the EDS analysis results in Table 1, the dark phase (spots 2, 4, 6, 9, 11) was identified as γ-TiAl, the light phase (spots 1, 3, 7, 8, 12) was identified as α_2-Ti_3Al and the bright phase (spots 5 and 10) was identified as Mo-rich γ-TiAl.

The densities of the specimens determined on the basis of Archimedes' method are listed in Table 2. The relative densities obtained by dividing the measured density values to the calculated theoretical density values give information about the porosity amount of the specimens. Depending on the material composition, the densities of γ-TiAl and α_2-Ti_3Al phases vary between 3.7-3.9 and 4.1−4.7 g cm^{-3}, respectively [30]. Since the specimens synthesized in this study were composed of γ-TiAl and α_2-Ti_3Al phases, the densities measured were also observed to be in the range of the density values of these two phases. It was also found that the relative densities of Mo-added specimens were lower compared to other specimens.

In TiAl based intermetallic produced by powder metallurgy method, the large difference between Ti and Al diffusion rate causes Kirkendall effect during sintering [25,31]. When pressure is not applied during the sintering process, swelling and surface cracking occur in the material due to the formation of Kirkendall pores [31]. It should be noted that no swelling or surface cracking is observed in the specimens since the pressure is applied simultaneously with electric current during ECAS. The microhardness values of the specimens are listed in Table 3. As shown in Table 2, the additions of Cr, Mn and Mo caused some increase in the hardness of the specimens. Similar results were observed by other authors [32,33].

3.2. Analysis of weight change measurements

Materials should be resistant not only to high temperatures but also to conditions requiring periodically activation and deactivation. Therefore, cyclic oxidation testing is applied to determine and/or improve the properties of materials operating at high temperatures. The weight change per surface unit area was obtained by dividing the weight difference of the specimens weighed before and after oxidation (m_2-m_1) with the surface area of the specimen. Weight changes are the sum of the weight gain caused by the formation of oxides and the weight loss caused by exfoliation [34]. Therefore, the weight changes are positive or negative values. Oxidation behavior of the specimens was evaluated as following:

$$\Delta W = \frac{(m_2 - m_1)}{A} \quad (3)$$

Where ΔW is the weight change per unit area (mg cm^{-2}), m_1 is the initial weight (mg), m_2 is the weight after each cycle (mg), A is the total surface area of the specimens (cm^2). The calculated equations and correlation coefficients for weight change curves are shown in Table 4.

The oxidation behavior of the intermetallics at 700, 800, and 900 °C can be seen from the weight change plot with respect to time (Fig. 5(a−c)). Fig. 5(a−c) shows that increasing oxidation temperature and time accelerated the weight change, indicating the temperature and time have a significant effect on the oxidation rate of the materials. It can be seen from Fig. 4 (a) that the weight change of Ti−48Al after 180 h of oxidation at 700 °C is approximately 3.7 mg cm^{-2}. In this temperature, the weight change of the specimen with at.% 2Cr addition was found to be about 2.5 times higher than the base specimen. It has been reported in many papers that the addition of Cr at low concentration (<at.% 4) increases the oxidation rate of TiAl-based intermetallic [17,35−37]. Therefore at.% 2Cr addition is thought to cause an increase in the weight change of the specimens. The harmful effect of Cr can be attributed to the doping effect, which would cause an increase in the concentration of O^{2-} vacancies, which are responsible for oxygen diffusion and thus the growth rate of the TiO_2 [38]. At 700 °C, it was observed that the weight change of Ti−48Al−2Mn compared to that of Ti−48Al was about two times. However, it can be seen from Fig. 5 (a) that the weight change of the specimen with at.% 2Mn addition (~8 mg cm^{-2}) at the same temperature is less than that of the specimen with at.% 2Cr addition (~10 mg cm^{-2}). Mn is also known to have a reducing effect on the oxidation resistance of TiAl-based intermetallic [5,35]. However, in this study, it is thought that the

Please cite this article as: Y. Garip, O. Ozdemir, A study of the cycle oxidation behavior of the Cr/Mn/Mo alloyed Ti−48Al−based intermetallics prepared by ECAS, Journal of Alloys and Compounds, https://doi.org/10.1016/j.jallcom.2019.152818

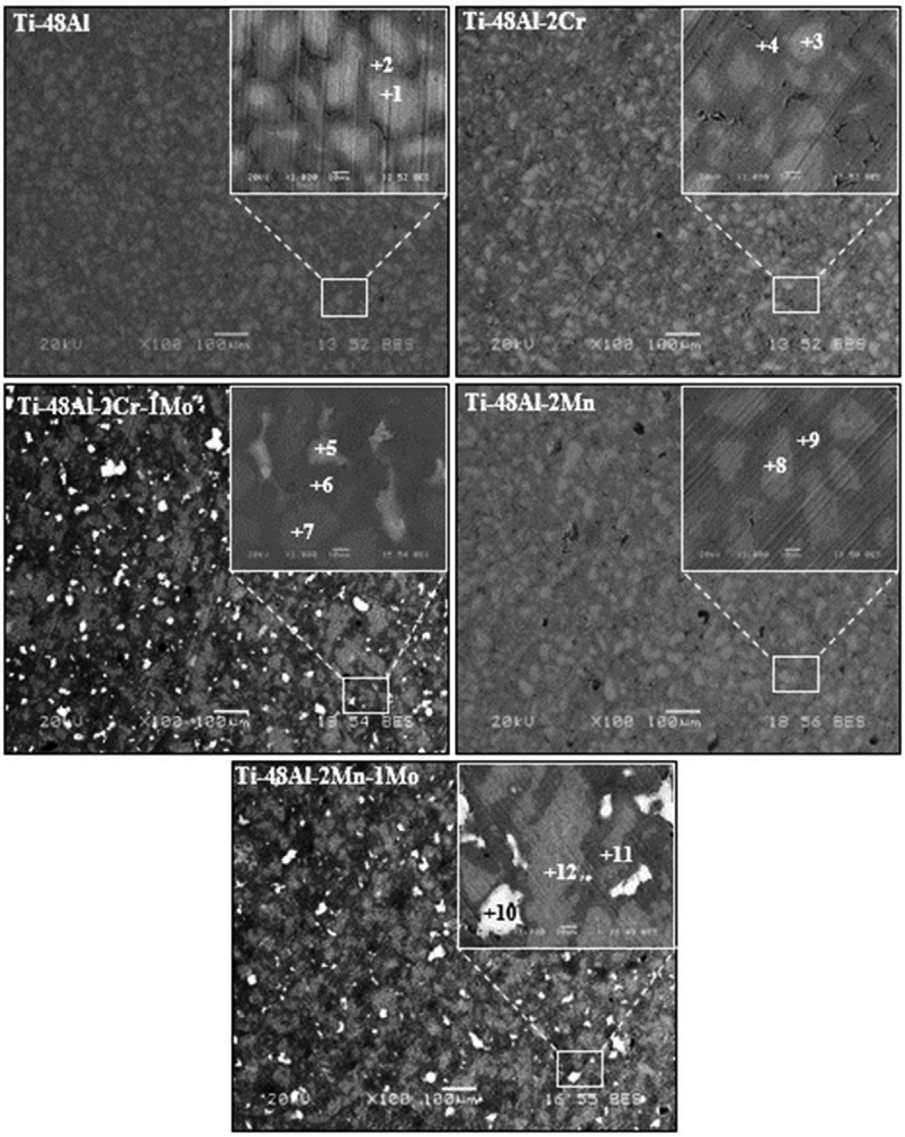

Fig. 4. SEM images of the microstructures of synthesized TiAl-based intermetallics. Insets show higher magnification of the marked area.

Table 1
Chemical compositions (at. %) of spots shown in Fig. 4.

Spot	Ti	Al	Cr	Mn	Mo
1	71.6	28.4	–	–	–
2	44.7	55.3	–	–	–
3	67.9	30.8	1.3	–	–
4	39.7	58.1	2.2	–	–
5	48.9	41.2	2.4	–	7.5
6	40.4	56.9	1.8	–	0.9
7	54.3	43.5	1.6	–	0.6
8	72.9	24.8	–	2.3	–
9	39.7	58.5	–	1.8	–
10	40.8	51.9	–	1.1	6.2
11	44.5	53.5	–	1.9	0.8
12	57.9	39.5	–	2.2	0.4

oxidation behavior of specimens is more sensitive to Cr element. The results are consistent with those observed by Kekare and Aswath [36]. These authors investigated the oxidation behavior of at.% Ti–48Al-1.5Cr and Ti–48Al-1.4Mn alloys at 704 °C and reported that the Mn-added alloy exhibited superior oxidation resistance compared to the other. When the addition of Mo is concerned, it can be seen that a decrease in the weight change of the specimens occurs. For example, the weight changes of Ti–48Al–2Cr–1Mo and Ti–48Al–2Cr after oxidation at 700 °C were 9.8 and 3.6 mg cm^{-2}, respectively.

In their oxidation test at 800–1000 °C, Anada and Shida [39] investigated the effect of Mo added to at.% Ti–48Al alloy in different amounts (up to at.% 2.4) on the oxidation resistance of the alloy and found that weight change decreased with the increase of Mo addition. Additionally, it was reported that the relative effectiveness of added alloying elements followed the order: Mo > Nb > Si [40]. The role of Mo in improving the oxidation resistance of TiAl-based intermetallic can be explained by the Wagner-Hauffe rule [41,42]. As a result of the substitution of a cation with higher valence electron than Ti (such as Mo^{+6},W^{+6},Nb^{+5}) with Ti^{+4} in the TiO_2 lattice, the oxygen vacancies concentration decreases and the growth of TiO_2 is prevented.

As shown in Fig. 5(b and c), as the diffusion rate of anions and cations increases due to the increase in oxidation temperature, the weight changes in the specimens increase as well. It was reported

Please cite this article as: Y. Garip, O. Ozdemir, A study of the cycle oxidation behavior of the Cr/Mn/Mo alloyed Ti–48Al–based intermetallics prepared by ECAS, Journal of Alloys and Compounds, https://doi.org/10.1016/j.jallcom.2019.152818

Table 2
Densities of specimens prepared by ECAS.

Specimens	Measured density (g cm^{-3})	Theoretical density (g cm^{-3})	Relative density (%)
Ti–48Al	3.82	3.88	98.4
Ti–48Al–2Cr	3.90	3.97	98.2
Ti–48Al–2Cr–1Mo	3.98	4.10	97
Ti–48Al–2Mn	3.87	3.95	98
Ti–48Al–2Mn–1Mo	4.01	4.12	97.3

Table 3
Micro-hardness values of the specimens.

Specimens	Micro-hardness ($Hv_{0.1}$)
Ti–48Al	344 ± 18
Ti–48Al–2Cr	352 ± 14
Ti–48Al–2Cr–1Mo	368 ± 25
Ti–48Al–2Mn	347 ± 17
Ti–48Al–2Mn–1Mo	359 ± 21

that the addition of Cr is the most harmful element to the oxidation resistance of at.% Ti–48Al alloy at 800 °C but this effect decreases as the amount of Cr increases [37]. It can be seen from Fig. 5 (b) that Ti–48Al–2Cr exhibits the poorest oxidation resistance at 800 °C. At all oxidation temperatures, Ti–48Al–2Cr–1Mo and Ti–48Al–2Mn–1Mo exhibited similar oxidation behavior. In the paper [21], the oxidation properties of at.% Ti–48Al–2Cr–2Nb and Ti–48Al–2Mn–2Nb alloys were investigated and the latter alloy was found to have relatively superior oxidation resistance. Apparently, Mn was a more effective alloying element in comparison to Cr in terms of oxidation resistance at 700–900 °C.

In addition, a rapid weight change occurred in the specimens during the first 24 h of oxidation at 700, 800 and 900 °C. Due to the high affinity of Ti and Al to oxygen, it is believed that the nucleation and growth of oxides on the surface of the specimens at the initial stage of oxidation occur rapidly. On the other hand, the fact that no oxide film yet formed on the free surface, can cause oxidation reactions to occur fastly. However, after 72 h of oxidation, a significant decrease in the oxidation rate of the specimens, especially in the Mo-added ones, was observed. This phenomenon can be attributed to two reasons: the first is that an alumina-rich layer is formed in the oxide scale, which is consistent with the cross-sectional SEM images of the oxide scale. Secondly, as oxidation proceeds, the diffusion distance of species increases due to the increase in oxide scale thickness. Therefore, depending on the nature of parabolic kinetics, the rate of oxidation is initially high but decreases with time.

The power law equation was used to determine what laws the weight change curves obey [42]:

$$\left(\Delta\frac{W}{A}\right)^{n} = k_n t \tag{4}$$

Where k_n is the rate constant, t is the oxidation time and n is the power exponent. As shown in Fig. 6, in order to identify oxidation kinetics, a linear regression was performed on a double logarithm plot of the weight change data versus oxidation time. Determination of the kinetic rate equation is based on the parameter n (1/R), which is the inverse of the slope obtained from the linear regression in Fig. 6. After n values were determined, oxidation rate constants (kn) are obtained by regression analysis of the weight change per surface area versus time. Calculated values of n and k_n for the oxidized specimens are listed in Table 5. These n values of 1, 2, and 3, corresponding to linear, parabolic, and cubic kinetics, respectively. In the current study, the oxidation of specimens nearly followed parabolic kinetics ($n \approx 2$) at the investigated temperatures. However, oxidation kinetics of Ti–48Al and Ti–48Al–2Cr follows a linear rate law at 900 °C for 180 h. In the linear kinetics, the oxidation rate is constant with time as shown in Fig. 5 (c). A linear kinetic curve shows that formed oxide scale is non-protective due to the presence of pores and micro cracks in the oxide scale [43]. It can be seen that the kn values of the specimens increase with the increase in oxidation temperature. This means that a higher oxidation rate constant value reflects a higher oxidation rate. At the same time, the addition of Mo reduced the oxidation rate constants of the samples, i.e. retarded the oxidation. For example, at 800 °C, the oxidation rate constants of Ti–48Al–2Cr and Ti–48Al–2Cr–1Mo were 0.9328 and 0.3164 mg^{n} cm^{-2n} h^{-1}, respectively. This suggests that Mo has a beneficial influence on enhancing the oxidation resistance of the specimens.

The oxidation rate constant (k_n) is a function of temperature and it was estimated by the Arrhenius Eq. [17]:

$$k_n = k_o \ \exp\left(\frac{-Q}{RT}\right) \tag{5}$$

Where k_o is the frequency factor, Q is the activation energy, R is the gas constant (8.314 J/mol K) and T is the temperature (K). Activation energy for oxidation is calculated by plotting the natural logarithm of the rate constant (Ln (k_n)) versus the inverse of the temperature (1/T). Linear regression is performed and the slope is multiplied by the gas constant to obtain the activation energy for oxidation.

As presented in Fig. 7, the specimen with higher activation energy has a steeper slope. The calculated activation energy values for the oxidation of the studied specimens were 91 kJ mol^{-1} (Ti–48Al), 50 kJ mol^{-1} (Ti–48Al–2Cr), 116 kJ mol^{-1} (Ti–48Al–2Cr–1Mo), 59 kJ mol^{-1} (Ti–48Al–2Mn), 114 kJ mol^{-1} (Ti–48Al–2Mn–1Mo). The higher activation energy for oxidation shows that oxygen atoms diffuse more difficult in the specimens. The activation energy values of several TiAl based alloys with various alloying elements

Table 4
Statistical parameters for oxidized TiAl based specimens obtained by regression analysis of weight changes vs. time plot from Fig. 5

Materials	700 °C		800 °C		900 °C	
	ΔW	R^2	ΔW	R^2	ΔW	R^2
Ti–48Al	$0.9096\ t^{0.280}$	0.99	$1.4515\ t^{0.2694}$	0.99	$0.2179\ t^{1.0029}$	0.99
Ti–48Al–2Cr	$1.0187\ t^{0.4550}$	0.98	$0.7304\ t^{0.5516}$	0.98	$0.3706\ t^{0.9309}$	0.99
Ti–48Al–2Cr–1Mo	$0.2497\ t^{0.5241}$	0.99	$1.4460\ t^{0.3020}$	0.98	$2.6223\ t^{0.2555}$	0.99
Ti–48Al–2Mn	$1.8966\ t^{0.9830}$	0.97	$5.4462\ t^{0.1299}$	0.98	$0.9222\ t^{0.5827}$	0.99
Ti–48Al–2Mn–1Mo	$0.2524\ t^{0.4927}$	0.96	$2.0341\ t^{0.1954}$	0.97	$6.3920\ t^{0.090}$	0.98

Please cite this article as: Y. Garip, O. Ozdemir, A study of the cycle oxidation behavior of the Cr/Mn/Mo alloyed Ti–48Al–based intermetallics prepared by ECAS, Journal of Alloys and Compounds, https://doi.org/10.1016/j.jallcom.2019.152818

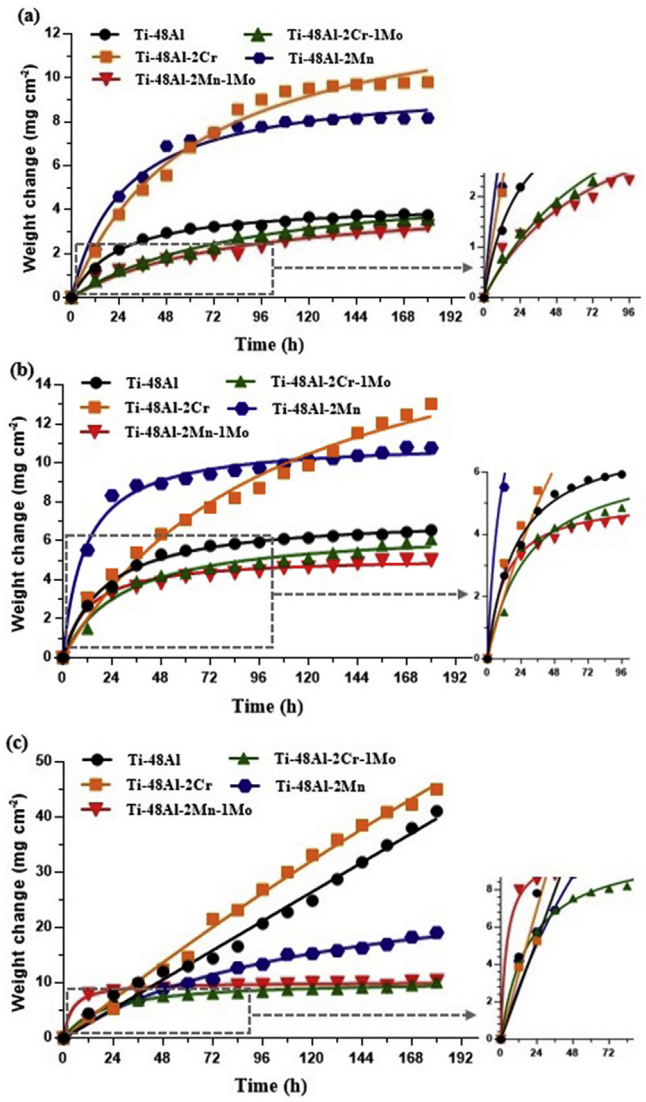

Fig. 5. Plots of weight change vs. oxidation time for TiAl-based intermetallics, (a) 700 °C, (b) 800 °C and (c) 900 °C.

reported in the literature are as follows [44]: 138 kJ mol^{-1} (Ti–48Al–2Cr–2Nb), 114 kJ mol^{-1} (Ti–48Al–2Cr–2Nb-0.5W), 146 kJ mol^{-1} (Ti–48Al–2Cr–2Nb–1W). When the activation energy values of the investigated alloys are compared with those reported, this difference can be attributed to oxidation temperature, alloy composition, atmosphere type, surface finishing and production method. It should be noted that both oxidation rate constant (see Table 5) and activation energy considerably affected by the alloying elements. As mentioned before, Cr has a deleterious effect on the oxidation behavior of the TiAl based alloys, however, in this study, the doping effect of Mo counterbalanced the deleterious effect due to Cr. It can be suggested that the kinetic parameters emphasize the positive role of Mo addition.

3.3. XRD analysis

To detect the phases present in the oxide scales after exposure, the specimens were scanned by X-ray diffraction (XRD). Fig. 8(a–c) displays XRD analysis of the oxide scales formed on TiAl based specimens after 180 h at 700–900 °C. XRD analysis reveals that oxide scales have consisted of TiO_2 and Al_2O_3 (corundum) phases at all test temperatures after exposure of 180 h. The mixed structure Al_2O_3 and TiO_2 was formed on the surfaces as they have similar Gibbs free energy [42]. Since the formed oxide scale was not thick or uniform, the peaks of Ti_3Al and TiAl phases in the matrix were also detected at 700 °C. However, after exposure to 800 and 900 °C, the Ti_3Al was not observed in the XRD patterns. The reason is that the Ti_3Al oxidized to TiO_2 with increasing temperature. This is consistent with the reported results [17]. When exposure temperature was increased, weak diffraction signals corresponding the TiAl phase were detected in the XRD patterns. It was also observed that the intensity of TiO_2 increased. This revealed that the oxide scale thickness increases with oxidation temperature.

3.4. Surface morphology of the oxidized specimens

The surface morphologies of the oxide scales after oxidation at 700 °C for 180 h are shown in Fig. 9 and the chemical composition corresponding to the spots is listed in Table 6. EDS analysis indicates that the formed oxide scales in the specimens consist of TiO_2 and Al_2O_3, which is in accordance with the XRD results shown in Fig. 8. As can be seen from Fig. 9, the surfaces of the oxidized Ti–48Al, Ti–48Al–2Cr and Ti–48Al–2Cr–1Mo specimens were composed of dark (spot 1, 3 and 5) and grey (spot 2, 4 and 6) phase regions. It was observed that the dark regions in the scales composed of oxide clusters. It can be seen that the oxide clusters were a mixture of Ti and Al oxides and they have more oxygen content than other regions.

In the present study, with regard to the formed oxide cluster, it may be suggested that due to the different Ti content of TiAl and Ti_3Al phases, the same oxidation rate cannot be induced in different phase regions. According to the detailed SEM images, the oxide clusters consisted of fine oxides with almost spherical-shaped crystals. It can be clearly discerned that oxidation products formed on the surfaces of Ti–48Al–2Cr and Ti–48Al–2Mn were more than those of the other specimens. This is also supported by the weight change curves of the specimens in Fig. 4 (a). However, as seen in Fig. 9, the surface of the oxidized Ti–48Al–2Mn–1Mo specimen was relatively smoother. Additionally, the presence of grinding signs can be visible on the surfaces because the oxide scale is not formed completely on the surface of the specimens after exposure of 700 °C.

Fig. 10 shows the SEM images of specimens' surfaces subjected to oxidation at 800 °C for 180 h. It was reported that the oxide scale formed on the surfaces of TiAl based intermetallics at high temperatures. After the initial stage, the TiO_2 forms the outer oxide layer because faster growing TiO_2 grains cover to Al_2O_3 grains [14]. From the SEM images of the surfaces (Fig. 10) and EDS analysis (Table 7), it can be seen that analysis spots (except spot 5) corresponded to large grained TiO_2. The size of TiO_2 grains formed on the surface of Ti–48Al–2Cr was larger compared to that of other specimens. The reason for the formation of the relatively large-grained TiO_2 on the Ti–48Al–2Cr can be attributed to the oxygen vacancy concentration increased by doping effect of Cr, namely, Cr showed a harmful effect on the oxidation resistance of the specimens. However, as to the specimens with Mo addition, it was observed in Fig. 10 that formed TiO_2 grains were smaller. It is considered that Mo is an effective element in terms of oxidation resistance. As a result, the further oxidation of the specimens was prevented by addition of Mo alloying element. This result is consistent with reports in Ref. [46]. The higher magnification of marked areas (Fig. 10) shows that titanium oxide grains formed on the surfaces seem to be polyhedron structure. Additionally, as can

Please cite this article as: Y. Garip, O. Ozdemir, A study of the cycle oxidation behavior of the Cr/Mn/Mo alloyed Ti–48Al–based intermetallics prepared by ECAS, Journal of Alloys and Compounds, https://doi.org/10.1016/j.jallcom.2019.152818

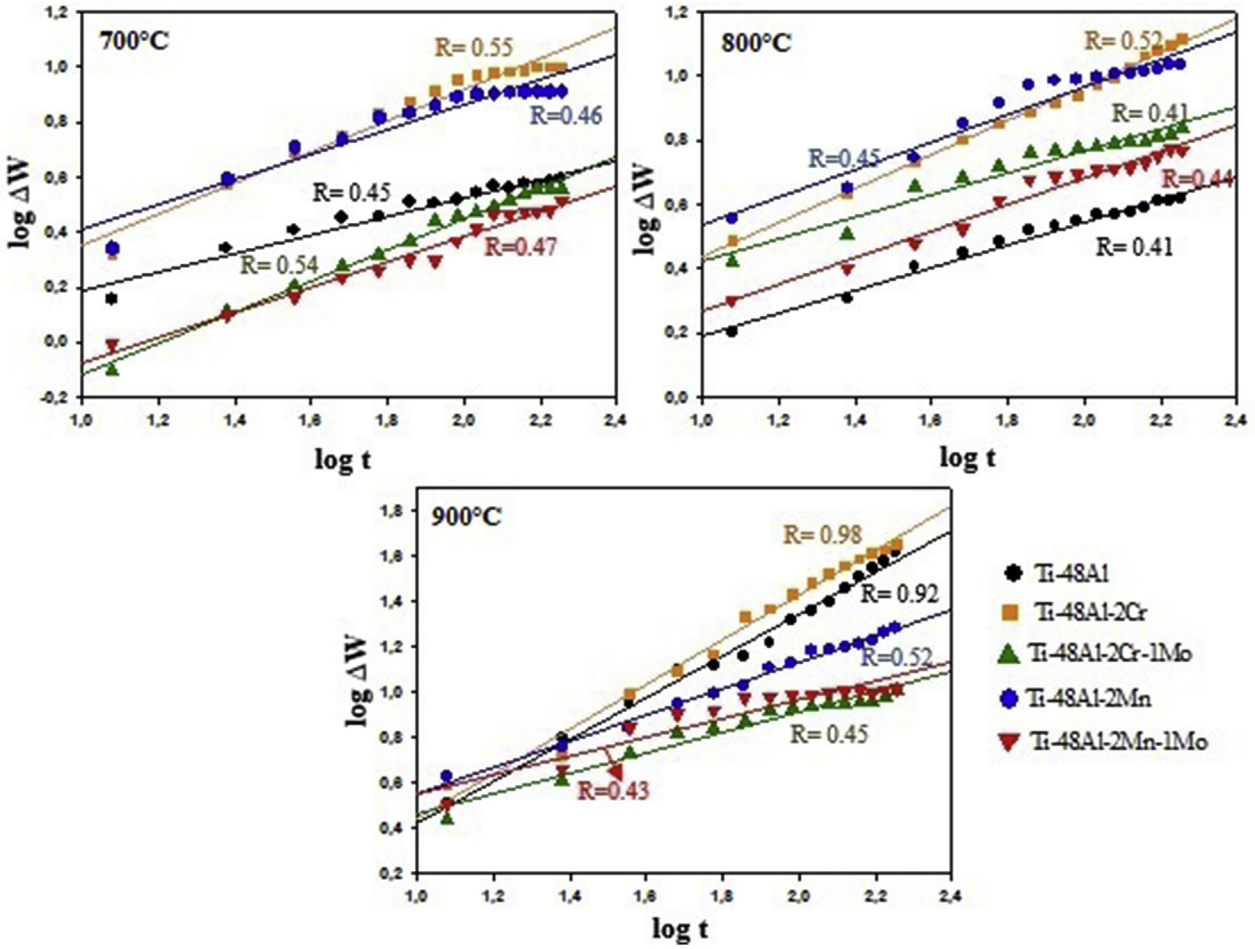

Fig. 6. Log-log plots of the weight change versus time for TiAl-based intermetallics at 700, 800 and 900 °C for 180 h.

Table 5
Calculated values of n and oxidation rate constants (kn, $mg^n\ cm^{-2n}\ h^{-1}$) for the oxidized specimens at 700–900 °C.

Materials	700 °C		800 °C		900 °C	
	n	k_n	n	k_n	n	k_n
Ti–48Al	2.22	0.1006	2.44	0.1708	1.08	0.7050
Ti–48Al–2Cr	1.81	0.3256	1.92	0.9328	1.02	0.905
Ti–48Al–2Cr–1Mo	1.85	0.0643	2.27	0.3164	2.22	0.7272
Ti–48Al–2Mn	2.17	0.5219	2.22	0.7216	1.92	1.8980
Ti–48Al–2Mn–1Mo	2.12	0.0691	2.27	0.2288	2.32	0.7566

be seen from 7 (b) the higher peaks of the TiO_2 suggest the relatively thicker oxide scale.

Fig. 11 displays the SEM images of surfaces of the oxidized specimens at 900 °C for 180 h and the EDS analysis results are listed in Table 8. As oxidation temperature increases from 800 °C to 900 °C, it was observed that the specimen surface is completely covered with randomly oriented TiO_2 grains. The mean size of TiO_2 grains for the best specimen and the worst specimen was approx. 3 μm and 15 μm, respectively, which was bigger than that of oxides formed at 800 °C and the grains had a pillar-like structure. This indicates that TiO_2 grains incline to grow as the exposure temperature increase. Differently, the oxide grains formed at the surface of the Ti–48Al–2Mn–1Mo specimen appear to be close to the globular shape and were finer in comparison with the others. It was reported that more plasticity of the oxide scale was guaranteed by the fine structure and it enhances resistance to exfoliation of the oxide scale [42]. It should be noted that the growth direction of the

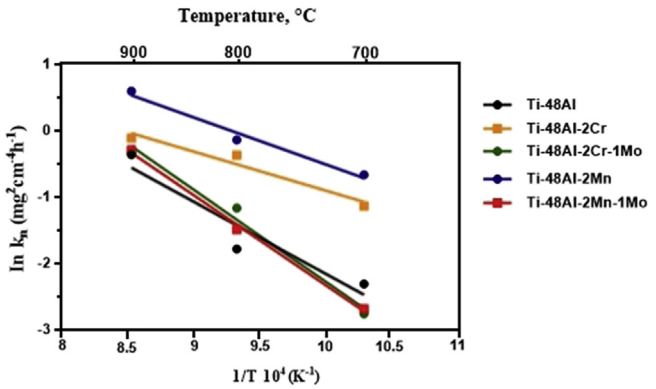

Fig. 7. Calculation of the activation energies for the oxidation of TiAl based specimens.

TiO_2 grains is perpendicular to the surface at 800 °C, whereas the grains tend to grow laterally at 900 °C. As shown in Fig. 5 (c), the data of the weight change per unit area increased by the increase in exposure temperature and this is also confirmed by the SEM surface examinations of the oxidized specimens.

3.5. Cross-sectional morphology of the oxidized specimens

The cross-sectional microstructures of the TiAl based specimens oxide scale formed at 800 °C and 900 °C for 180 h are depicted in

Please cite this article as: Y. Garip, O. Ozdemir, A study of the cycle oxidation behavior of the Cr/Mn/Mo alloyed Ti–48Al–based intermetallics prepared by ECAS, Journal of Alloys and Compounds, https://doi.org/10.1016/j.jallcom.2019.152818

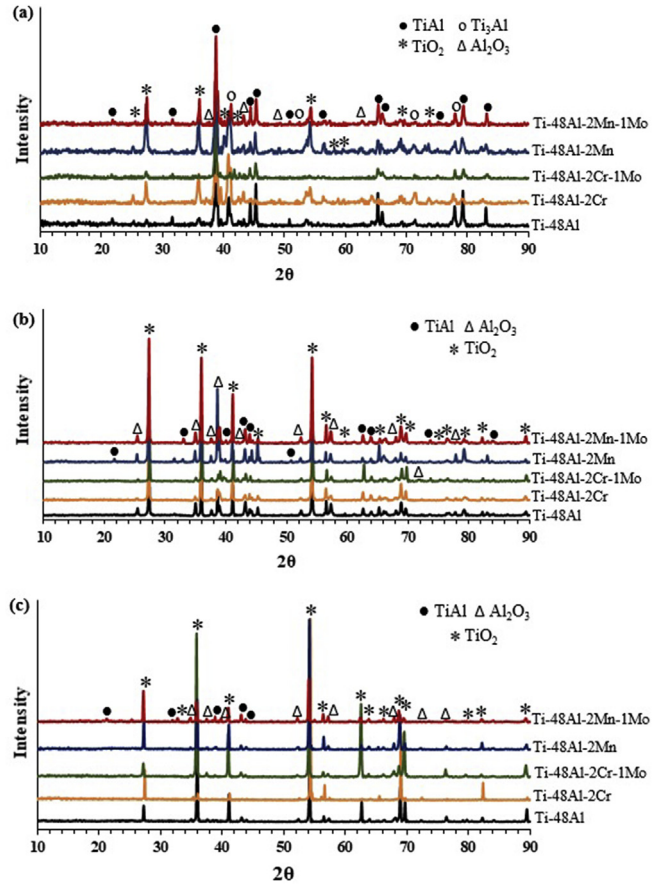

Fig. 8. XRD patterns of the specimens after oxidation for 180 h: (a) 700 °C, (b) 800 °C and (c) 900 °C.

Fig. 12 and EDS analysis results are listed in Table 9. As the oxide scales formed on the specimens at 700 °C were quite thin, they have not been presented. SEM images of the cross-sectional microstructures show that the multi-layered of oxide scale structure formed on the specimens is similar to that of formed on the TiAl alloys. The EDS analysis in Table 9 indicated that the oxide scale consists of outer layer TiO_2 (spots 1, 5, 8, 12, 15, 18, 22, 25, 29 and 32), an intermediate Al_2O_3 layer (spots 2, 6, 9, 13, 16, 19, 23, 26, 30 and 33) and an inner TiO_2+Al_2O_3 mixed layer (spots 3, 7, 10, 14, 17, 20, 24, 27, 31 and 34). It was reported that the outer TiO_2 layer was grown by the outward diffusion of Ti ions and intermediate Al_2O_3 layer was grown by inward diffusion of oxygen and the outward diffusion of Al ions [14,45]. Additionally, as Al_2O_3 is permeable for both O and Ti ions, the inner mixed layer and the outer TiO_2 layer would continue to grow. Consequently, as it can be seen from Fig. 8, inner TiO_2+Al_2O_3 mixed layer and an outer TiO_2 layer are respectively formed on the beneath and above the Al_2O_3 layer.

When the oxide scale reaches a certain thickness, the rate of oxidation is controlled via diffusion of O^{2-} and metal ions (Ti^{4+} and Al^{3+}) in TiO_2 layer. The oxidation temperature increase accelerates the diffusion of anions and cations and as a result of this oxide scale grows faster than that of the 800 °C. It is noted that the plasticity ability of the scale is lower when an alloy subjected to oxidation for a longer time and formed oxide scale on the alloy reaches a critical thickness. Additionally, there was a sublayer (spot 4, 11, 21, 28, 35) consisting of an Al-depleted region and its composition corresponded to α_2-Ti_3Al phase (at.% Al 22–39).

It was observed that the presence of oxide scales with varied thickness formed on the specimens. Therefore, the mean oxide

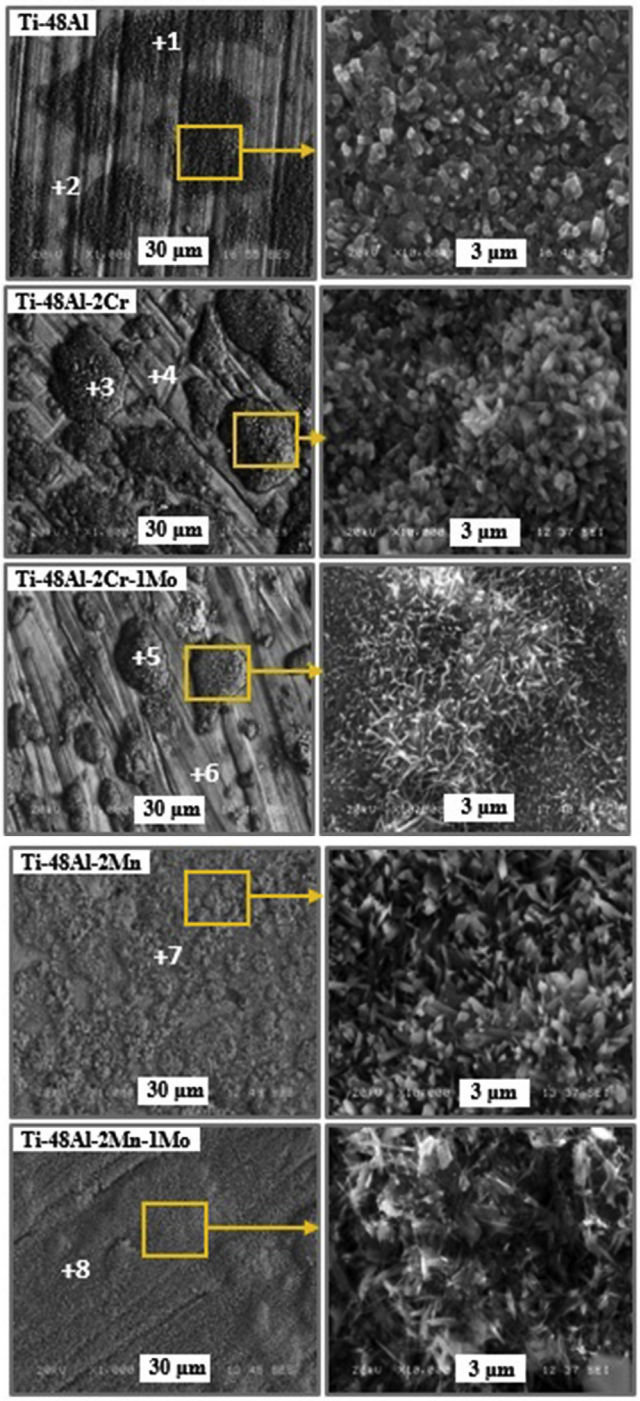

Fig. 9. SEM surface morphologies of oxidized specimens at 700 °C for 180 h.

scale thickness was measured by taking the average of thickness of three different regions in the cross-sectional SEM images. When considering the thicknesses of the oxide scales formed on specimens with or without Mo addition, the oxide growth in Ti–48Al–2Cr–1Mo and Ti–48Al–2Mn–1Mo are suppressed in comparison with other specimens. For example, exposed to the same oxidation conditions at 900 °C, thicknesses of the oxide scales formed on Ti–48Al–2Mn and Ti–48Al–2Mn–1Mo specimens were respectively 75.8 ± 3 μm and 36.3 ± 1 μm. It can be concluded that the influence of Mo on the oxidation behavior of specimens is really important. However, since oxidation kinetics of Ti–48Al (n value of 1.08) and Ti–48Al–2Cr (n value of 1.02) follows a linear

Please cite this article as: Y. Garip, O. Ozdemir, A study of the cycle oxidation behavior of the Cr/Mn/Mo alloyed Ti–48Al–based intermetallics prepared by ECAS, Journal of Alloys and Compounds, https://doi.org/10.1016/j.jallcom.2019.152818

Table 6
The chemical composition of the oxide scales formed at 700 °C.

Spot	Element (at.%)					
	Ti	Al	Cr	Mn	Mo	O
1	19.4	16.1	–	–	–	64.5
2	23.5	28.3	–	–	–	48.2
3	24.8	13.2	0.3	–	–	59.7
4	28.8	31.8	0.6	–	–	38.8
5	28.4	17.4	0.2	–	0.2	53.8
6	24.2	29.2	0.4	–	0.3	45.9
7	21.5	18.1	–	0.3	–	60.1
8	20.1	16.7	–	0.9	0.7	61.6

rate law at 900 °C, the quite thick oxide scales formed on the surfaces of the specimens were observed (Fig. 12). Due to the fact that the Al_2O_3 layer was beneath the TiO_2 layer in oxide scale, the absence of a significant increase in Al_2O_3 peak intensity at 900 °C can be attributed to the presence of thicker titanium oxide layer compared to 800 °C.

Besides, there was a crack parallel to the interface in the oxide scale formed on the Ti–48Al–2Mn at 900 °C. It is considered that the crack is produced during the heating and cooling process and is stem from stress induced between the substrate and the oxide scale. It is also found that curling deformation in oxide scale formed on the same specimen at 800C. The reason for the formation of curling deformation can be attributed to the release of developed stress (compressive and tensile stresses).

EDS analysis indicates that there were accumulated Mo elements in the sublayers. Similar results were reported by other authors [14]. The likely reasons are that Mo has bigger ion radii (0.65 Å) compared to the other ions and is a slow diffuser in Ti alloys. It is worth noting that oxygen partial pressure varied through the oxide scale thickness, namely, it is the lowest at the oxide/substrate interface and the highest at the air/oxide interface. In this regard, when the partial oxygen pressure required for the oxidation of Mo is reached in the oxide scale, it will be oxidized to form its stable oxide. It was observed that there were voids in the outer TiO_2 layer formed on the Ti–48Al and Ti–48Al–2Cr at 900 °C (Fig. 12). This observation was also obtained by Taniguchi et al. [47]. According to these authors, the voids were formed in consequence of the initial growth of TiO_2 crystals nearly perpendicular to the surface and keeping their lateral growth till meeting each other. It is important to highlight that voids deteriorate the adherence between the scale and substrate. Moreover, the diffusion rate of O_2 is rapid through the voids, resulting in further oxidation.

It is well known that the oxidation behaviors of TiAl alloys at elevated temperatures mostly depend on the protective properties of the oxide scale formed on their surfaces. Unfortunately, TiAl alloys do not form protective Al_2O_3 film while they form TiO_2, which has a porous morphology that does not form long term oxidation protection [14]. In the current study, the oxidation of TiAl based specimens resulted in an outer TiO_2 layer, as seen in Fig. 11. It is known that TiO_2 is an n-type oxide showing non-stoichiometry TiO_{2-x}, where x could vary up to ~0.008 depending on temperature and oxygen partial pressure. The oxygen deficiency of TiO_2 is compensated with oxygen vacancies and titanium interstitials in the lattice [48].

The formation of oxygen vacancies can be represented by using the Kroger-Vink notation, as following:

$$O_O = V_{\ddot{O}} \frac{1}{2} O_2 + 2e^{\prime} \quad (6)$$

Where O_O is an oxygen anion on a normal site, $V_{\ddot{O}}$ is an oxygen vacancy, $e^{\prime}$ is an electron. The $V_{\ddot{O}}$ is regarded as a major defect in

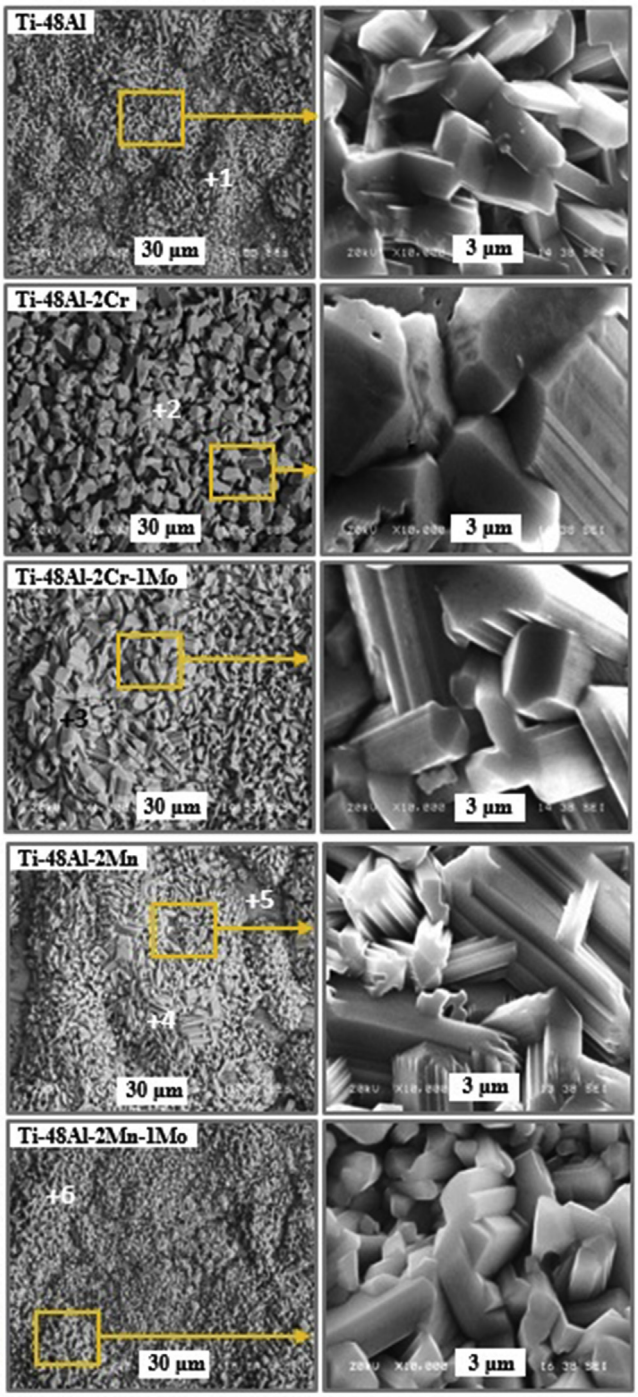

Fig. 10. SEM surface morphologies of oxidized specimens at 800 °C for 180 h.

Table 7
The chemical composition of the oxide scales formed at 800 °C.

Spot	Element (at.%)					
	Ti	Al	Cr	Mn	Mo	O
1	29.1	0.4	–	–	–	70.5
2	26.9	0.7	0.1	–	–	72.3
3	29.1	0.2	0.1	–	0.1	70.5
4	27.6	0.9	–	0.2	–	71.3
5	16.4	28.5	–	0.9	–	54.2
6	25.3	0.7	–	0.3	0.6	73.1

Please cite this article as: Y. Garip, O. Ozdemir, A study of the cycle oxidation behavior of the Cr/Mn/Mo alloyed Ti–48Al–based intermetallics prepared by ECAS, Journal of Alloys and Compounds, https://doi.org/10.1016/j.jallcom.2019.152818

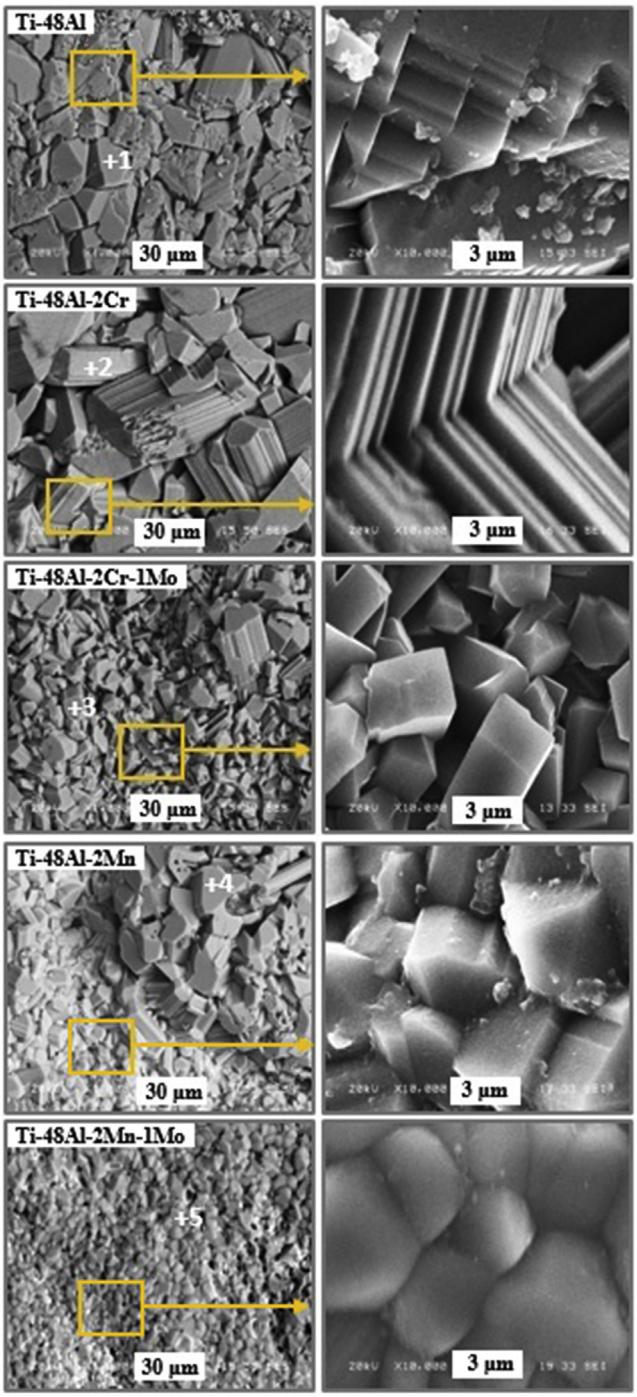

Fig. 11. SEM surface morphologies of oxidized specimens at 900 °C for 180 h.

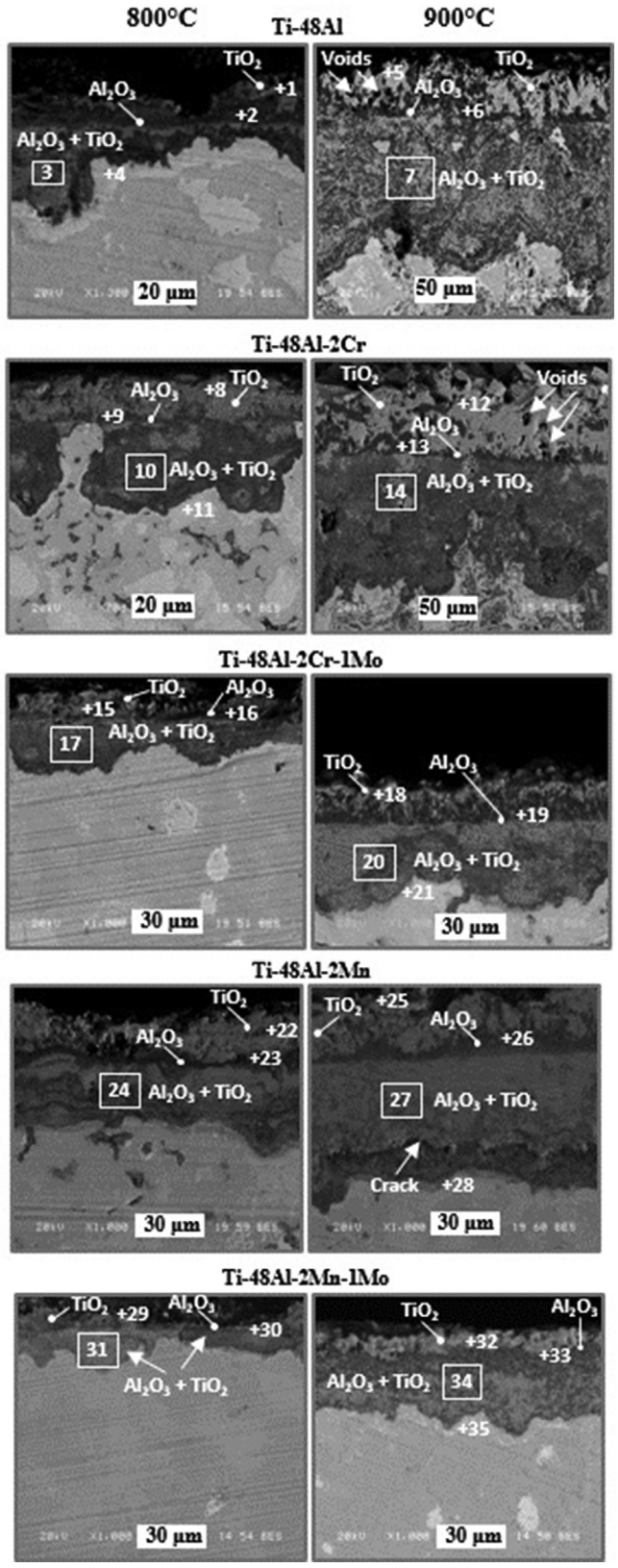

Fig. 12. SEM images of the cross-sectional microstructures of oxide scale formed on the specimens at 800 °C and 900 °C for 180 h.

Table 8
The chemical composition of the oxide scales formed at 900 °C.

Spot	Element (at.%)					
	Ti	Al	Cr	Mn	Mo	O
1	36.5	0.4	–	–	–	63.1
2	41.9	0.3	0.1	–	–	57.7
3	25.6	0.9	0.2	–	0.1	73.2
4	32.1	0.2	–	0.5	–	67.2
5	29.6	0.2	–	0.4	0.1	69.7

Please cite this article as: Y. Garip, O. Ozdemir, A study of the cycle oxidation behavior of the Cr/Mn/Mo alloyed Ti–48Al–based intermetallics prepared by ECAS, Journal of Alloys and Compounds, https://doi.org/10.1016/j.jallcom.2019.152818

Table 9
The chemical composition of spots 1–35 shown in Fig. 12.

Spot	Element (at.%)					
	Ti	Al	Cr	Mn	Mo	O
1	25.7	2.6	–	–	–	71.7
2	8.1	39.7	–	–	–	52.1
3	19.5	21.3	–	–	–	59.2
4	60.3	32.1	–	–	–	7.6
5	29.1	0.7	–	–	–	70.2
6	1.9	46.1	–	–	–	52
7	16.7	22.7	–	–	–	60.6
8	33.1	0.7	0.2	–	–	66
9	9.2	32.2	0.1	–	–	58.5
10	15.3	24.7	0.2	–	–	59.8
11	59.6	32.9	1.3	–	–	6.2
12	27.6	0.3	0.1	–	–	72
13	2.3	42.5	0.5	–	–	54.7
14	14.6	28.4	0.9	–	–	56.1
15	24.6	0.9	0.1	–	0.1	74.3
16	11.2	31.3	0.5	–	0.2	56.8
17	18.9	23.4	0.4	–	0.2	57.1
18	29.8	0.6	0.1	–	0.1	69.4
19	7.2	36.4	0.3	–	0.2	55.9
20	20.1	18.8	0.6	–	0.4	60.1
21	56	33.9	1.4	–	3.6	5.1
22	27.3	0.8	–	0.1	–	71.8
23	5.4	33.1	–	0.4	–	61.1
24	18.8	25.2	–	0.9	–	55.1
25	31.3	1.1	–	0.1	–	67.5
26	3.6	36.8	–	0.5	–	59.1
27	20.2	19.6	–	0.9	–	59.3
28	57.8	34.2	–	1.8	–	6.2
29	25.6	3.7	–	0.3	0.1	70.3
30	4.3	33.6	–	0.4	0.3	61.4
31	22.6	19.4	–	0.3	0.4	57.3
32	29.5	1.8	–	0.2	0.1	68.4
33	2.9	37.5	–	0.3	0.3	59
34	17.2	24.1	–	0.5	0.4	57.8
35	52.6	30.3	–	1.6	8.7	6.8

TiO_2. If the doped cations with higher valence than Ti occupy normal Ti-sites, it is expected to inhibit the formation of oxygen vacancies. Based on the above considerations, the electroneutrality condition can be written as:

$$(Me_{Ti}^{\cdot}) = (V_{\ddot{O}}) + (e^{\prime}) \tag{7}$$

where the $Me_{Ti}^{\cdot}$ denotes Me^{5+} cation on a normal Ti-site, $V_{\ddot{o}}$ is an oxygen vacancy, $e^{\prime}$ is an electron. The net charge on the left and right hand sides of the reaction must be equal. Addition of Mo can potentially form MoO_3 with a cation of valence +6. In addition, Mo and Ti have similar ion radius. The incorporation of Mo^{6+} into the TiO_2 lattice would decrease concentration of oxygen vacancies by the following defect reaction:

$$MoO_3 + V_{\ddot{O}} = Mo_{Ti}^{\cdot\cdot} + 3O_O \tag{8}$$

$$MoO_3 = Mo_{Ti}^{\cdot\cdot} + 2O_O + \frac{1}{2}O_2(g) + 2e^{\prime} \tag{9}$$

$Mo_{Ti}^{\cdot\cdot}$ is the Mo^{6+} ion occupying a normal Ti^{4+} site and carries +2 charge with respect to the TiO_2 lattice. Two excess positive charges must be compensated by formation of electrons with negative charges (Eq. (9)) or annihilation of oxygen vacancies (Eq. (8)), which are responsible for oxygen diffusion. This phenomenon can be explained by the doping effect of Mo^{6+} ions. It is worth noting that the outer TiO_2 layer is formed by outward diffusion of Ti^{4+} ions and inward diffusion of oxygen vacancies from an outer part of the oxide scale. As a result, it is considered that the doping of Mo in the defect structure of TiO_2 contributes to improvement of the oxidation resistance. This result is consistent with the one reported by Wu et al. [5].

In contrast, addition of Cr having lower valence than Ti introduces oxygen vacancies and thus, the growth rate of TiO_2 increases. The reaction for the formation of oxygen vacancies is given by:

$$Cr_2O_3 = Cr_{Ti}^{\prime} + V_{\ddot{O}} + 3O_O \tag{10}$$

$$Cr_2O_3 + 2e^{\prime} + \frac{1}{2}O_2(g) = Cr_{Ti}^{\prime} + 4O_O \tag{11}$$

The dopant cation, $Cr^{3+,}$ occupies a normal Ti^{4+} site and carries −1 charge, 2 $Cr_{Ti}^{\prime}$. This negative charge is compensated by formation of oxygen vacancies (Eq. (10)) or annihilation of electrons (Eq. (11)). Therefore, the increase in the concentration of oxygen vacancy can lead to an increased oxidation rate of the alloys. It is reasonable to conclude that the Cr has a harmful influence on the oxidation behavior of TiAl alloys. However, in this study, the detrimental effect of Cr seems to have been overshadowed by the doping effect of Mo. It is worth noting that beneficial or detrimental effects of alloying elements depend on several factors such as the microstructure of alloy, chemical composition, exposure temperatures and concentration of the dopants.

Ping et al. reported that the formation energy of oxygen vacancy in TiO_2 lattice is affected by the added alloying elements [41]. It was proposed by these authors that the oxygen diffusion rate (D) is proportional to the vacancy concentration and can be expressed in the following equation:

$$D = AC_V r \tag{12}$$

C_V is the vacancy concentration, A is the crystal lattice related factor and r is the successful jump frequency of the atom. The vacancy concentration can be expressed by the following equation [41]:

$$CV = B\exp\left(\frac{\Delta E}{k_B T}\right) \tag{13}$$

ΔE is the energy required for vacancy formation, k_B is the Boltzmann constant and T is the temperature. Based on Eq. (13), the oxygen vacancy concentration in TiO_2 lattice can be reduced by increasing the formation energy of oxygen vacancy. In this regard, fast diffusion paths for O_2 transport will be reduced and inhibited further oxidation of TiAl. Their calculations suggest that Mo, Zr, Hf, Nb, and W alloying elements increase the energy required for oxygen vacancy formation in TiO_2 lattice [41]. Therefore, Mo can be regarded as an important alloying element in respect to oxidation resistance of TiAl.

When thermodynamic and kinetic aspects of oxidation of TiAl are considered, the probable chemical reactions occurring at a high temperature in the oxidizing environment are:

$$\frac{1}{2}Ti_{(s)} + O_{2(g)} = TiO_{(s)} \tag{14}$$

$$TiO_{(s)} + \frac{1}{2}O_{2(g)} = TiO_{2(s)} \tag{15}$$

$$2Al_{(s)} + \frac{3}{2}O_{2(g)} = Al_2O_{3(s)} \tag{16}$$

Thermodynamic calculations yielded the affinity energy of

Please cite this article as: Y. Garip, O. Ozdemir, A study of the cycle oxidation behavior of the Cr/Mn/Mo alloyed Ti–48Al–based intermetallics prepared by ECAS, Journal of Alloys and Compounds, https://doi.org/10.1016/j.jallcom.2019.152818

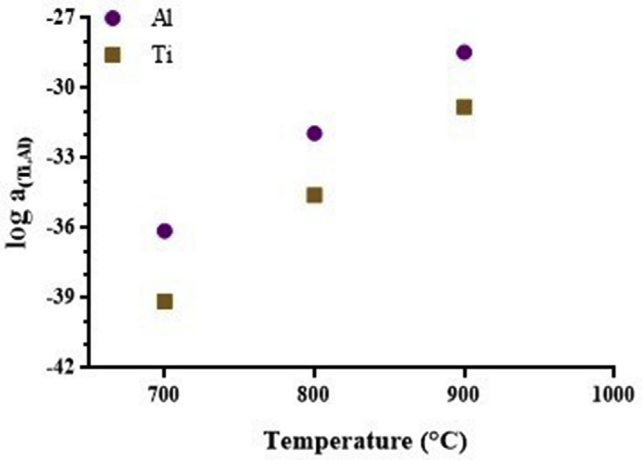

Fig. 13. The minimum activities of Al and Ti required to form Al_2O_3 and TiO_2 for 700–900 °C.

Al_2O_3 formed by Al and oxygen is −30.00 eV, and that of TiO formed by Ti and O is −28.27 eV. Due to the fact that affinity energy of TiO and Al_2O_3 is very close, the selective oxidation of Al to form Al_2O_3 is difficult. However, as the TiO is an unstable oxide, it will rapidly oxidize to stable oxide TiO_2 and thus it is usually occurred rather than TiO. In addition, the affinity energy of TiO_2 formed by Ti and O is −54.99 eV [35]. One of the reasons for poor oxidation resistance of TiAl alloys can be attributed to the above considerations. However, Al concentration plays a key role to form a continuous and protective Al_2O_3 layer. It was reported that Al concentration required to form an Al_2O_3 is at.% 60–70 for exposure in air [46]. The minimum activities of Ti and Al in the materials should also be considered. Details about the activity calculations can be found in our previous study [17]. It can be seen from Fig. 13 that minimum activities of Al and Ti are required to form their parent oxides. Fig. 13 indicates that the favor the formation of TiO_2. Moreover, kinetic calculations in our previous study show that Ti diffusivity is more than an order of magnitude bigger than Al diffusivity in the TiAl for 800 °C [17].

As it can be seen from Fig. 11, the surfaces of the specimens were covered by the titanium oxide layer which has rapid growth kinetics. In other words, it can be concluded that the cross-sectional microstructures of oxide scales were supported by thermodynamic and kinetic considerations.

4. Conclusions

In this study, electric current activated sintering (ECAS) technique, enabling the preparation of materials with superior properties compared to traditional sintering techniques, is used. The cyclic oxidation behavior of TiAl based specimens produced by ECAS method was investigated at 700, 800 and 900 °C for 180 h.

As a result of the experimental investigations, the following conclusions can be drawn:

1. The produced TiAl-based specimens consist of a two-phase ($\alpha_2+\gamma$) microstructures, as desired. The relative density and micro hardness values of the specimens ranged between % 98.4–97 and 344 ± 18–368 ± 25 $Hv_{0.1}$, respectively.
2. The morphology of the oxide scale formed on the specimens and oxidation kinetics were significantly affected by oxidation temperature and alloying elements. While all specimens nearly followed parabolic oxidation kinetics at 700 and 800 °C, Ti–48Al and Ti–48Al–2Cr followed linear oxidation kinetics at 900 °C (estimated n values of 1.08 and 1.02, respectively)
3. The oxidation products were Al_2O_3 (corundum) and TiO_2 after oxidation at 700–900 °C for 180 h. However, the increase in the exposure temperature increases the intensity of TiO_2 phase.
4. The growth rate of the outer TiO_2 layer was suppressed by the doping effect of Mo and the further oxidation of the specimens was prevented.
5. Mn was a more effective alloying element in comparison to Cr in terms of oxidation resistance at 700–900 °C.
6. The composition and structure of the oxide scales formed on the specimens were similar. After exposure at 800 and 900 °C, a triple-layered oxide scale developed on the surfaces consisted of $TiO_2+Al_2O_3/Al_2O_3/TiO_2$ from the matrix to surface. However, the Al_2O_3 layer was more pronounced in specimens with Mo alloying element. The critical thickness of the oxide scale was not exceeded by means of Mo addition and as a result of this, the resistance of cracking and exfoliating are enhanced
7. The activation energy values for the oxidation of the best (Ti–48Al–2Cr–1Mo) and the worst (Ti–48Al–2Cr) specimen were 50 kJ mol^{-1} and 116 kJ mol^{-1}, respectively.

References

[1] V.A.C. Haanappel, M.F. Stroosnijder, The effect of ion implantation on the oxidation behaviour of TiAl-based intermetallic alloys at 900°C, Surf. Coat. Technol. 105 (1998) 147–154, https://doi.org/10.1016/S0257-8972(98)00472-1.
[2] S.Y. Chang, The isothermal and cyclic oxidation behavior of a titanium aluminide alloy at elevated temperature, JMEPEG 16 (4) (2007) 508–514, https://doi.org/10.1007/s11665-007-9066-7.
[3] Y. Xiong, C. Guan, S. Zhu, F. Wang, Effect of enamel coating on oxidation and hot corrosion behaviors of Ti-24Al-14Nb-3V alloy, JMEPEG 15 (5) (2006) 564–569, https://doi.org/10.1361/105994906X136151.
[4] H.-R. Jiang, Z.-L. Wang, W.-S. Ma, X.-R. Feng, Z.-Q. Dong, L. Zhang, Y. Liu, Effects of Nb and Si on high temperature oxidation of TiAl, Trans. Nonferrous Metals Soc. China 18 (2008) 512–517, https://doi.org/10.1016/S1003-6326(08)60090-4.
[5] Y. Wu, S.K. Hwang, K. Hagihara, Y. Umakoshi, Isothermal oxidation behavior of two-phase TiAl–Mn–Mo–C–Y alloys fabricated by different processes, Intermetallics 14 (2006) 9–23, https://doi.org/10.1016/j.intermet.2005.02.014.
[6] Z. Yao, M. Marek, NaCl-induced hot corrosion of a titanium aluminide alloy, Mater. Sci. Eng. A 192–193 (1995) 994–1000, https://doi.org/10.1016/0921-5093(95)03345-9.
[7] C.-Z. Qiu, Y. Liu, L. Huang, B. Liu, W. Zhang, Y.-H. He, B.-Y. Huang, Tuning mechanical properties for β (B2)-containing TiAl intermetallics, Trans. Nonferrous Metals Soc. China 22 (2012) 2593–2603, https://doi.org/10.1016/S1003-6326(11)61505-7.
[8] K. Kothari, R. Radhakrishnan, N.M. Wereley, Advances in gamma titanium aluminides and their manufacturing techniques, Prog. Aerosp. Sci. 55 (2012) 1–16, https://doi.org/10.1016/j.paerosci.2012.04.001.
[9] B.P. Bewlay, S. Nag, A. Suzuki, M.J. Weimer, TiAl alloys in commercial aircraft engines, Mater. A. T. High. Temp. 33 (4–5) (2016) 549–559, https://doi.org/10.1080/09603409.2016.1183068.
[10] A. Brotzu, F. Felli, D. Pilone, Effect of alloying elements on the behaviour of TiAl based alloys, Intermetallics 54 (2014) 176–180, https://doi.org/10.1016/j.intermet.2014.06.007.
[11] B.G. Kim, G.M. Kim, C.J. Kim, Oxidation behaviour of TiAl-X (X=Cr, V, Si, Mo or Nb) intermetallics at elevated temperature, Scr. Mater. 33 (1995) 71117–71125, https://doi.org/10.1016/0956-716X(95)00327-R.
[12] D. Pilone, F. Felli, Isothermal oxidation behaviour of TiAl-Cr-Nb-B alloys produced by induction melting, Intermetallics 26 (2012) 36–39, https://doi.org/10.1016/j.intermet.2012.03.008.
[13] Z. Tang, F. Wang, W. Wu, Effect of a sputtered TiAlCr coating on hot corrosion resistance of gamma-TiAl, Intermetallics 7 (1999) 1271–1274, https://doi.org/10.1016/S0966-9795(99)00044-8.
[14] D.J. Kim, D.Y. Seo, H. Saari, T. Sawatzky, Y.-W. Kim, Isothermal oxidation behavior of powder metallurgy beta gamma TiAl-2Nb-2Mo alloy, Intermetallics 19 (2011) 1509–1516, https://doi.org/10.1016/j.intermet.2011.05.027.
[15] J. Małecka, W. Grzesik, A. Hernas, An investigation on oxidation wear mechanisms of Ti-46Al-7Nb-0.7Cr-0.1Si-0.2Ni intermetallic-based alloys, Corros. Sci. 52 (2010) 263–272, https://doi.org/10.1016/j.corsci.2009.09.015.
[16] S. Grasso, Y. Sakka, G. Maizza, Electric current activated/assisted sintering (ECAS): a review of patents 1906–2008, Sci. Technol. Adv. Mater. 10 (2009) 1–24, https://doi.org/10.1088/1468-6996/10/5/053001.
[17] Y. Garip, O. Ozdemir, Comparative study of the oxidation and hot corrosion

Please cite this article as: Y. Garip, O. Ozdemir, A study of the cycle oxidation behavior of the Cr/Mn/Mo alloyed Ti–48Al–based intermetallics prepared by ECAS, Journal of Alloys and Compounds, https://doi.org/10.1016/j.jallcom.2019.152818

behaviors of TiAl-Cr intermetallic alloy produced by electric current activated sintering, J. Alloy. Comp. 780 (2019) 364–377, https://doi.org/10.1016/j.jallcom.2018.11.324.
[18] R. Orrù, R. Licheri, A.M. Locci, A. Cincotti, G. Cao, Consolidation/synthesis of materials by electric current activated/assisted sintering, Mater. Sci. Eng. R 63 (2009) 127–287, https://doi.org/10.1016/j.mser.2008.09.003.
[19] D.B. Lee, K.B. Park, M. Nakamura, Effects of Cr and Nb on the high temperature oxidation of TiAl, Met. Mater. Int. 8 (3) (2002) 319–326, https://doi.org/10.1007/BF03186102.
[20] L.K. Wu, W.Y. Wu, J.L. Song, G.Y. Hou, H.Z. Cao, Y.P. Tang, G.Q. Zheng, Enhanced high temperature oxidation resistance for γ-TiAl alloy with electrodeposited SiO_2 film, Corros. Sci. 140 (2018) 388–401, https://doi.org/10.1016/j.corsci.2018.05.025.
[21] D.J. Kim, D.Y. Seo, Q. Yang, H. Saari, T. Sawatzky Y.-W. Kim, Isothermal oxidation behaviour of beta gamma powder metallurgy TiAl-4Nb-3Mn alloys, Can. Metall. Q. 50 (4) (2011) 416–424, https://doi.org/10.1179/000844311X13112418376129.
[22] D. Mudgal, S. Singh, S. Prakash, Cyclic hot corrosion behavior of superni 718, superni 600, and superco 605 in sulfate and chloride containing environment at 900°C, Metallogr. Microstruct. Anal. 4 (2015) 13–25, https://doi.org/10.1007/s13632-014-0182-0.
[23] C.-L. Zhang, X.-J. Wang, X.-M. Wang, X.-S. Hu, K. Wu, Fabrication, microstructure and mechanical properties of Mg matrix composites reinforced by high volume fraction of sphere TC4 particles, J. Magnes. Alloys 4 (4) (2016) 286–294, https://doi.org/10.1016/j.jma.2016.10.003.
[24] J. Sienkiewicz, S. Kuroda, R.M. Molak, H. Murakami, H. Araki, S. Takamori, K.J. Kurzyd1owski, Fabrication of TiAl intermetallic phases by heat treatment of warm sprayed metal precursors, Intermetallics 49 (2014) 57–64, https://doi.org/10.1016/j.intermet.2013.12.011.
[25] H.-W. Liu, K.P. Plucknett, Titanium aluminide (Ti-48Al) powder synthesis, size refinement and sintering, Adv. Powder Technol. 28 (2017) 314–323, https://doi.org/10.1016/j.apt.2016.10.001.
[26] Y. Sun, J. Haley, K. Kulkarni, M. Aindow, E.J. Lavernia, Influence of electric current on microstructure evolution in Ti/Al and Ti/$TiAl_3$ during spark plasma sintering, J. Alloy. Comp. 648 (2015) 1097–1103, https://doi.org/10.1016/j.jallcom.2015.07.079.
[27] U. Anselmi-Tamburini, J.E. Garay, Z.A. Munir, Fundamental investigations on the spark plasma sintering/synthesis process III. Current effect on reactivity, Mater. Sci. Eng. A 407 (2005) 24–30, https://doi.org/10.1016/j.msea.2005.06.066.
[28] J.R. Friedman, J.E. Garay, U. Anselmi-Tamburini, Z.A. Munir, Modified interfacial reactions in Ag–Zn multilayers under the influence of high DC currents, Intermetallics 12 (2004) 589–597, https://doi.org/10.1016/j.intermet.2004.02.005.
[29] A. Couret, G. Molénat, J. Galy, M. Thomas, Microstructures and mechanical properties of TiAl alloys consolidated by spark plasma sintering, Intermetallics 16 (2008) 1134–1141, https://doi.org/10.1016/j.intermet.2008.06.015.
[30] Y.W. Kim, Ordered intermetallic alloys, Part III: gamma titanium aluminides, JOM 46 (7) (1994) 30–39, https://doi.org/10.1007/BF03220745.
[31] J.B. Yang, W.S. Hwang, The preparation of TiAl-based intermetallics from elemental powders through a two-step pressureless sintering process, JMEPEG 7 (3) (1998) 385–392, https://doi.org/10.1361/105994998770347837.
[32] H. Usman, A. F. Mohd Noor, R. Astrawinata, The effects of Cr and Mo on the microstructure and mechanical properties of as-cast TiAl alloys, J. Eng. Technol. Sci. 45 (3) (2013) 294–306, https://doi.org/10.5614/j.eng.technol.sci.2013.45.3.6.
[33] Z. Nianlong, S. Zhiping, Effect of Cr on the microstructure and properties of high Nb-TiAl alloys prepared by hot-pressing sintering, in: International Conference on Materials Chemistry and Environmental Protection, 2016, https://doi.org/10.2991/meep-15.2016.1.
[34] S.Y. Park, D.Y. Seo, S.W. Kim, S.E. Kim, J.K. Hong, D.B. Lee, High temperature oxidation of Ti-46Al-6Nb-0.5W-0.5Cr-0.3Si-0.1C alloy, Intermetallics 74 (2016) 8–14, https://doi.org/10.1016/j.intermet.2016.04.005.
[35] J. Dai, J. Zhu, C. Chen, F. Weng, High temperature oxidation behavior and research status of modifications on improving high temperature oxidation resistance of titanium alloys and titanium aluminides: a review, J. Alloy. Comp. 685 (2016) 784–798, https://doi.org/10.1016/j.jallcom.2016.06.212.
[36] S.A. Kekare, P.B. Aswath, Oxidation of TiAl based intermetallics, J. Mater. Sci. 32 (1997) 2485–2499, https://doi.org/10.1023/A:1018529829167.
[37] D. Kim, D. Seo, X. Huang, T. Sawatzky, H. Saari, J. Hong, Y.W. Kim, Oxidation behaviour of gamma titanium aluminides with or without protective coatings, Int. Mater. Rev. 237 (59) (2014) 297–325, https://doi.org/10.1179/1743280414Y.0000000034.
[38] J.W. Fergus, Review of the effect of alloy composition on the growth rates of scales formed during oxidation of gamma titanium aluminide alloys, Mater. Sci. Eng. A 338 (2002) 108–125, https://doi.org/10.1016/S0921-5093(02)00064-3.
[39] H. Anada, Y. Shida, Effect of Mo addition on the oxidation behavior of TiAl intermetallic compound, Mater. Trans. 36 (4) (1995) 533–539, https://doi.org/10.2320/jinstmet1952.58.7_746.
[40] O. Ostrovskaya, C. Badini, G. Baudana, E. Padovano, S. Biamino, Thermogravimetric investigation on oxidation kinetics of complex Ti-Al alloys, Intermetallics 93 (2018) 244–250, https://doi.org/10.1016/j.intermet.2017.09.020.
[41] F.P. Ping, Q.M. Hu, A.V. Bakulin, S.E. Kulkova, R. Yang, Alloying effects on properties of Al_2O_3 and TiO_2 in connection with oxidation resistance of TiAl, Intermetallics 68 (2016) 57–62, https://doi.org/10.1016/j.intermet.2015.09.005.
[42] X. Gong, R.R. Chen, H.Z. Fang, H.S. Ding, J.J. Guo, Y.Q. Su, H.Z. Fu, Synergistic effect of B and Y on the isothermal oxidation behavior of TiAlNb-Cr-V alloy, Corros. Sci. 131 (2018) 376–385, https://doi.org/10.1016/j.corsci.2017.12.013.
[43] I. Cvijović, M.T. Jovanović, D. Peruško, Cyclic oxidation behaviour of Ti_3Al-based alloy with Ni–Cr protective layer, Corros. Sci. 50 (2008) 1919–1925, https://doi.org/10.1016/j.corsci.2008.04.006.
[44] D.Y. Seo, T.D. Nguyen, D.B. Lee, Oxidation of powder metallurgy (PM) Ti–48% Al-2%Cr-2%Nb-(0-1%)W alloys between 800 and 1000°C in air, Oxid. Metals 74 (2010) 145–156, https://doi.org/10.1007/s11085-010-9203-9.
[45] P. Ouyang, G. Mi, P. Li, L. He, J. Cao, X. Huang, Non-isothermal oxidation behaviors and mechanisms of Ti-Al intermetallic compounds, Materials 12 (2019) 1–21, https://doi.org/10.3390/ma12132114.
[46] M. Naveed, A.F. Renteria, S. Weiß, Role of alloying elements during thermocyclic oxidation of β/γ-TiAl alloys at high temperatures, J. Alloy. Comp. 691 (2017) 489–497, https://doi.org/10.1016/j.jallcom.2016.08.259.
[47] V.A.C. Haanappel, R. Hofman, J.D. Sunderkiitter, W. Glatz, H. Clemens, M.F. Stroosnijder, The influence of microstructure on the isothermal and cyclic, oxidation behavior of Ti-48A1-2Cr at 800°C, Oxid. Metals 48 (3–4) (1997) 263–287, https://doi.org/10.1007/BF01670503.
[48] B. Sefer, Environment Related Surface Phenomena and Their Influence on Properties of Ti-6Al-4V and Ti-6Al-2Sn-4Zr-2Mo, Doctoral Thesis, 2016.

Please cite this article as: Y. Garip, O. Ozdemir, A study of the cycle oxidation behavior of the Cr/Mn/Mo alloyed Ti–48Al–based intermetallics prepared by ECAS, Journal of Alloys and Compounds, https://doi.org/10.1016/j.jallcom.2019.152818